Chinese Journal of Physics 61 (2019) 86–97

Contents lists available at ScienceDirect

Chinese Journal of Physics

journal homepage: www.elsevier.com/locate/cjph

Design of mid infrared high sensitive metal-insulator-metal plasmonic sensor

H. Ben salah*, A. Hocini, M.N. Temmar, D. Khedrouche

Laboratoire d'Analyse des Signaux et Systémes, Université Mohamed Boudiaf-M'sila, M'sila 28000, Algeria

ARTICLE INFO

Keywords:
Plasmonic sensor
Mid infrared
Surface plasmon polaritons(SPP)
Metal-insulator-metal (MIM) waveguide
Finite difference time domain (FDTD) method

ABSTRACT

In this paper, high sensitivity plasmonic refractive index sensor based on implanted cavities in Metal-Insulator-Metal (MIM) waveguide is designed and analyzed using two dimensional (2D) FDTD algorithm with perfectly matched layer boundary conditions. The dimensions of the introduced single and double cavities with rectangular defect are analyzed and simulated for the best sensor performance. The results reveal in linear correlation between the resonance wavelengths of the proposed defected cavities and the refractive index of the material under testing which is placed in the active region of the sensor. Also, simulation results show that the sensor resolution of refractive index, which depends on wavelength resolution of the detection system, can reach as high as 3.84×10^{-6} RIU, equivalentely to a sensitivity of 2602.5 nm/RIU, by taking the wavelength resolution of 0.01 nm.With the achieved optimum design by considering the tradeoff between the detected power, sensitivity and structure size, the transmittance level is enhanced by 118.08% compared to the first design. The proposed sensor can be used for different interesting applications such as identification of various materials including biosensor application, by proper design.

1. Introduction

The plasmonic sensor technology is a promising field as it can relieve the low precision and sensitivity problems. In addition, this plasmonics phenomenon, which occurs in nano-scale region, presents a new scope for device miniaturization that open extraordinary interesting applications in several other fields such as biosensors technology. Integrated biosensors not only have smaller size and weight but also have lower cost and promise for parallel monitoring and analysis. Further, they open up new prospects for high sensitive detection that were not fundamentally even possible with macroscopic sensor setups. In order to improve the emission intensity and to enhance the fluorescence detection to the sensitivity limit, it is found that controlling the local EM environment surrounding the emitter yields the desired objective. For the photoluminescence, the emission photon energy is critically related to the excited photon energy. As there exist mainly two categories of fluorescence, namely, downconversion and upconversion, It is also found that the spectral emission from an up conversion nanoparticle near plasmonic nanostructure can be modulated by controlling the configuration, composition of the plasmonic nanostructure and distance between the upconversion and surface. Dong and co-workers [1,2] Biosensors based on plasmonic phenomena are the most attractive candidates for integrated platform due to their potentially smaller size [3]. The existence of biomolecules in the active plasmonic region of the sensor results in a change of the refractive index (RI) at the metal-dielectric interface, As a result it modifies the propagation constant of the excited SPPs. Thus

* Corresponding author.
E-mail addresses: hocine.bensalah@univ-msila.dz (H. Ben salah), abdesselam.hocini@univ-msila.dz (A. Hocini), temmar.mohamed@univ-msila.dz (M.N. Temmar), djamel.khedrouche@univ-msila.dz (D. Khedrouche).

https://doi.org/10.1016/j.cjph.2019.07.006
Received 7 May 2019; Received in revised form 4 July 2019; Accepted 8 July 2019
Available online 04 August 2019

plasmonic sensors are suitable for both static sensing of biomolecules and real-time monitoring of biomolecular binding events.

Many devices are designed based on SPPs phenomena such as sensors [4], lasers [5], filters [6], Plasmon-induced transparency (PIT) structures [7] and logic gates [8]. To develop applications in biomedical and clinical fields, surface Plasmon resonance (SPR) sensors have been focused on for a series of applications such as proteins [9], DNA [10], and drugs [11] because of their high sensitivity, label-free nature, and fast reaction [12]. SPR based devices are widely employed in many applications including plasmonic demultiplexer [13], splitters [14], filters [15] and sensors [16]. Researchers have proposed different interesting approaches for the design of plasmonic refractive index sensors and applications [17–19]. Also, recent fabrication process of the proposed nanostructures patterns are introduced [20,21].

Several metal-insulator-metal (MIM) structures based on SPP phenomena are proposed for different applications such as optical filters [22] couplers [23] splitters [24] demultiplexers [25] switches [26] plasmonic filter [27], wavelength demultiplexing structures [28], Mach-Zehnder interferometers [29], sensors [30], nanolenses [31], splitters [32], and Y-shaped combiners [33], U-shaped waveguides [34], multimode-interferometers [35], couplers [36] and MachZehnder interferometers [37]. MIM structures have created a center of attention and numerous researches have been conducted in their analysis as they have a strong confinement of the electric field and a long propagation ranges [38] which maximize the interaction length of the field with the sensing substance. These properties are essential to increase the sensitivity of a sensing device.

Surface plasmon polariton SPPs are the excited waves on the metal surface due to the effect of the incident electromagnetic field in the contiguous dielectric and free electrons in metal. The ability of the SPPs to concentrate their energies in nanometer scale, by that means overcoming the classical optical diffraction limit, has made devices based on SPP very attractive for applications in densely integrated photonic devices [39]. Based on this phenomena, many interesting plasmonic structures are proposed by researchers for different sensing applications [40]

As the refractive index of any substance is related with different parameters, manufacturing of various sensors to measure temperature, pressure, humidity and concentration of chemicals [41] is applicable.

Plasmonic sensors currently present low sensitivity, which remains a challenge for researchers. However, for geometrically compact devices, one way to cross this challenge is by extending the interaction length which can be achieved by introducing hybrid cavities to facilitate re-circulation of optical and plasmonic resonance waves. Consequently, we can hypothesize that an appropriate MIM resonator structure in a sensor configuration will greatly increase the sensitivity of the resulting sensing device.

In the present contribution, design and enhancement of highly sensitive metal-insulator-metal plasmonic sensor in mid infrared spectral region is presented which can be used for several emerging sensing applications. In Section 2, MIM plasmonic structure is designed. In Section 3, simulation results for the designed MIM plasmonic structure are presented and investigated by studying the effects of different structural parameters. In Section 4, an enhanced MIM plasmonic structure is presented to improve the transmission level.In Section 5, simulation results for the designed enhanced MIM plasmonic structure are presented and investigated by studying the effects of the introduced structural parameters. Finally, Section 6, concludes the work.

2. MIM structure design

A schematic of the proposed MIM sensor is shown in Fig. 1. The sensor is composed of a slit, double teeth and a rectangular shaped defect inside the first tooth cavity. The slit width w is 50 nm, the dimensions of the double teeth are found after optimization to be

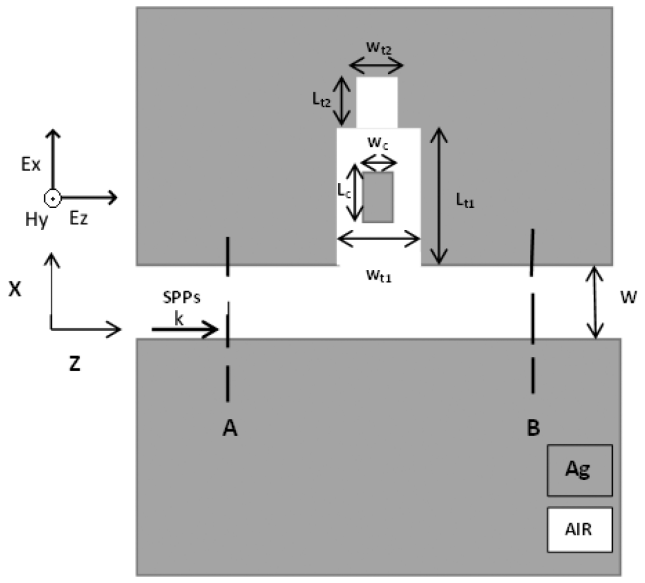

Fig. 1. 2-dimensional (2D) schematic of the presented metal-insulator-metal sensor coupled with rectangular defect in single cavity.

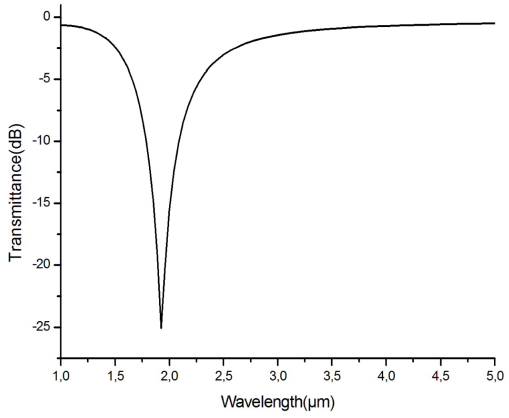

(a)

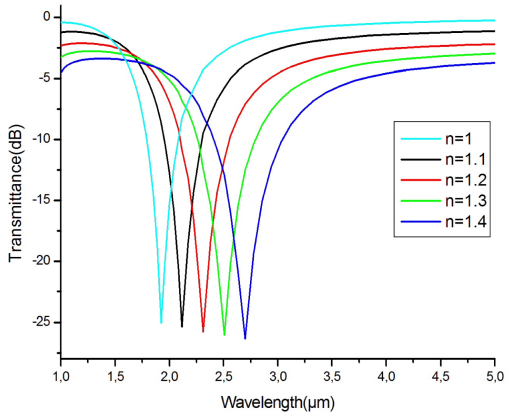

(b)

Fig. 2. The transmission spectra of MIM sensor coupled with rectangular defect in single cavity with dimensions $L_c = 75\,\text{nm}$ and $W_c = 30\,\text{nm}$ (a) filled with air (n = 1) in active region of the sensor (b) for different refractive indices.

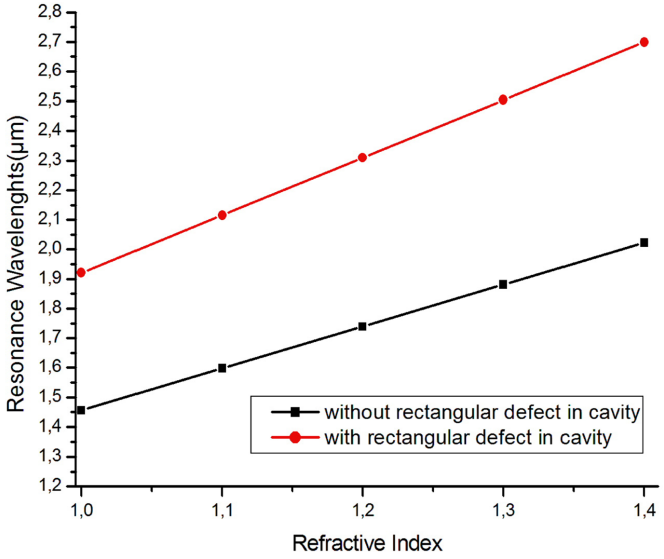

Fig. 3. The resonance wavelengths of MIM sensor coupled with rectangular defect in single cavity ($L_c = 75\,\text{nm}$, $W_c = 30\,\text{nm}$) and without rectangular defect in cavity versus the refractive index.

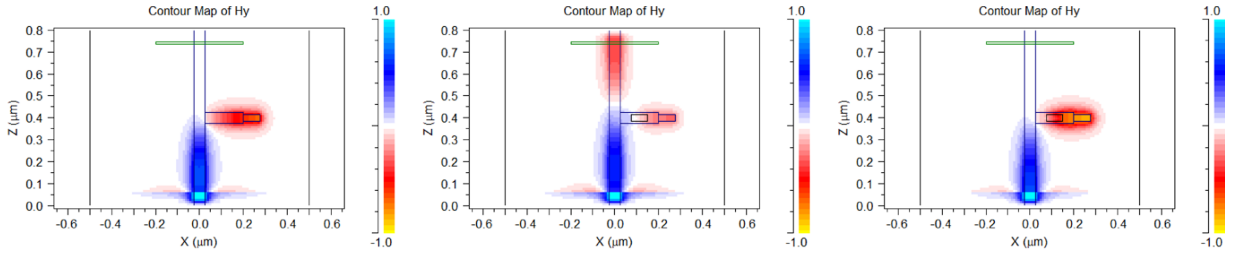

Fig. 4. The field distribution contours in the structure for (a) without tooth defect at resonance wavelength 1.46 μm. (b) with tooth defect $L_c = 75$ nm and $W_c = 30$ nm at wavelength 1.46 μm. (c) with tooth defect $L_c = 75$ nm and $W_c = 30$ nm at resonance wavelength 1.92 μm.

$W_{t1} = 50$ nm, $L_{t1} = 175$ nm, $W_{t2} = 30$ nm, and $L_{t2} = 75$ nm, respectively. The width of the MIM waveguide w is fixed to ensure that only the fundamental transverse magnetic (TM_0) mode is excited in the MIM waveguides [42]. The thickness of the proposed structure in the third dimension is much larger than the feature size in the plane of computation (2D). So, the effect of the substrate thickness on the achieved results can be neglected by mathematically assuming that the structure is infinite in the third dimension [43–45]. Thus, our simulations are all performed in 2D because of the achievable significant reduction in computational time without compromising with the accuracy of calculation. The rectangular defect in cavity has width W_c and length L_c which will be analyzed in next sections. the gray and white areas represent the silver (ϵ_m) layer and dielectric (ϵ_{in}), respectively.

Only the fundamental model (TM_0) can propagate along the waveguide because the width of the waveguide is much less than the incident wavelength. The dispersion relation of the fundamental TM_0 model in the plasmonic waveguide structure is given by [46].

$$\epsilon_{in} k_{z2} + \epsilon_m k_{z1} coth\left(-\frac{ik_{z1}}{2}\omega\right) = 0 \tag{1}$$

With k_{z1} and k_{z2} defined by momentum conservation

$$k_{z1}^2 = \epsilon_{in} k_0^2 - \beta^2 \tag{2}$$

$$k_{z2}^2 = \epsilon_m k_0^2 - \beta^2 \tag{3}$$

$$\epsilon_{in} = n^2 \tag{4}$$

Where ϵ_{in} is the dielectric constant of the insulator, β is the propagation constant and $k_0 = \frac{2\pi}{\lambda_0}$ is the free-space wave vector. The frequency-dependent complex relative permittivity ϵ_m of silver is characterized by the DrudeâLorentzian model with its dielectric constant [47]

$$\epsilon_m(\omega) = \epsilon_\infty - \frac{\omega_p^2}{\omega(\omega + i\gamma)} \tag{5}$$

where ϵ_∞ is the dielectric constant at the infinite angular frequency with a value of 3.7, ω_p is the bulk plasma frequency with a value of $1.38 \times 10^{16} Hz$, and $\gamma = 2.73 \times 10^{13} Hz$ is the electron collision frequency and ω is the angular frequency of the incident wave in vacuum [48,49]. In our simulation, the TM-polarized incident wave with inplane electric field components is directly coupled to the fundamental SPP mode [50]. The incident optical wave is converted into two parts, the transmitted wave and the reflected wave, by the resonator. Stable standing wave can only build up constructively within the resonator when the following resonant condition is satisfied [51,52]:

$$\Delta\varphi = 2\pi m,\ m = 1, 2, \ldots \tag{6}$$

The resonance wavelength can be described as follows [53]:

$$\lambda_m = \frac{2Sn_{eff}}{m - \frac{\varphi_{ref}}{\pi}} \tag{7}$$

Where S is the effective length of the resonator and n_{eff} denotes the real part of effective refractive index of the SPP, and φ_{ref} is the phase shift of SPP reflection at the resonator metal wall.

3. Simulation results

The two dimensional FDTD method using R-Soft CAD commercial software [51] with perfectly matched layers (PML) is applied in all sides to simulate the transmission spectrum of the structure. The grid sizes in the x and z directions are chosen as $\Delta x = \Delta z = 5$ nm, and the time step, derived by courant condition is $\Delta t = 0.95/c\sqrt{(\Delta x)^2 + (\Delta z)^2}$ [54] where c is the speed of light in free space. The input type is gaussian modulated continuous wave of TM polarization field. Two power monitors are set at A and B to detect the transmitted and incident powers. To calculate transmittance of the waveguide $T = P_{out}/P_{in}$ incident power of P_{in} and transmitted

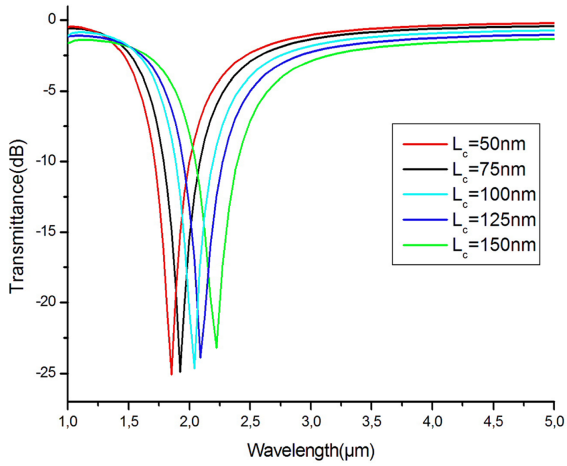

(a)

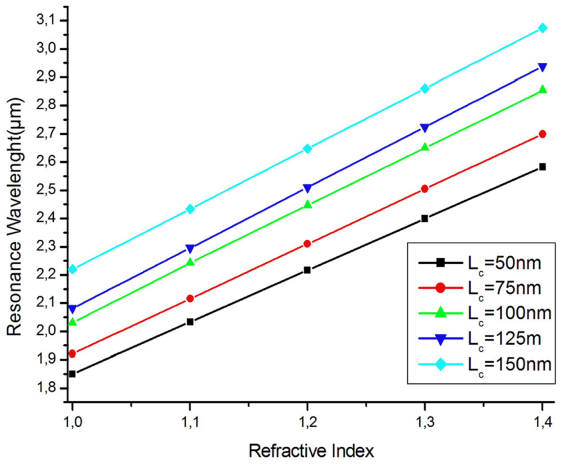

(b)

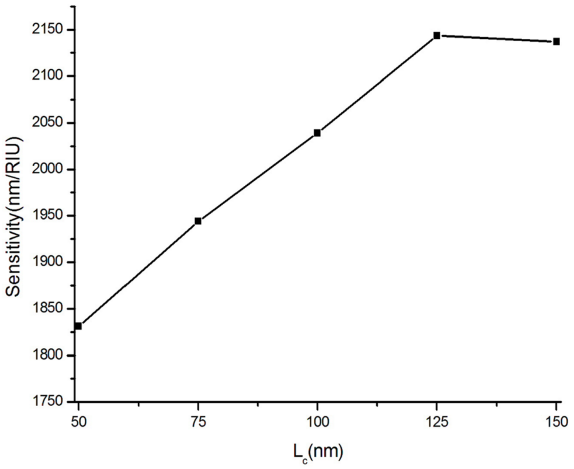

(c)

Fig. 5. Properties of MIM sensor coupled with rectangular defect in single cavity for various defect's rectangular lengths L_c = 50, 75, 100, 125 and 150 nm (a) The transmission spectra of refractive index 1 as functions of L_c (b) The resonance wavelengths versus the refractive index for different L_c (c) The sensitivity versus defect's rectangular length L_c.

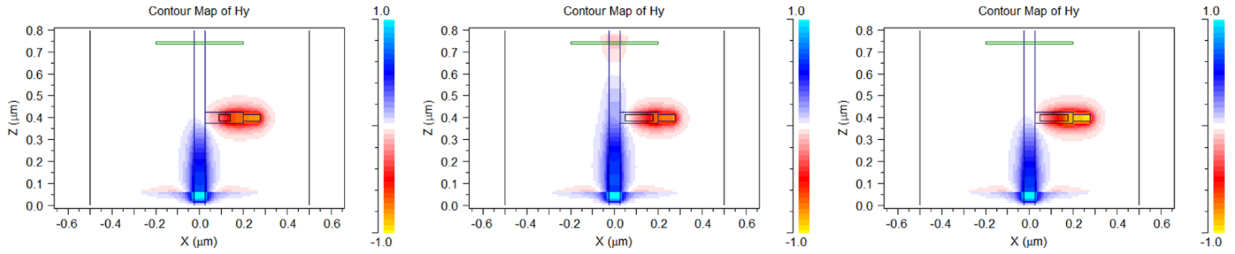

Fig. 6. The field distribution contours in the structure for tooth defect (a) tooth defect length $L_c = 50$ nm, width length $W_c = 30$ nm at resonance wavelength 1.85 μm. (b) $L_c = 125$ nm, $W_c = 30$ nm at wavelength 1.85 μm. (c) $L_c = 125$ nm, $W_c = 30$ nm at resonance wavelength 2.09 μm.

power of P_{out} are monitored at positions A and B, respectively.The effect of the simulation grids on the simulation is performed. The above FDTD calculations are repeated for smaller grid sizes and the accuracy is compared: if comparable accuracy is obtained, the results are accurate. If there is a large difference, then successively smaller grids are used until accurate results are found. This convergence process is done with the stop time to ensure accurate spectral results.

The transmission spectra of the plasmonic sensor filled with air ($n = 1$) and different refractive indices for rectangular defect in cavity of length $L_c = 75$ nm and width $W_c = 30$ nm is shown in Fig. 2. It can be seen that the minimum transmission of − 25.04 dB is achieved at 1921.15 nm for air. In Fig. 2(b), it is obviously observed the shift in minima wavelength toward longer wavelength as the refractive index is increased.This is due to the correlation relation between the effective refractive index and the resoncance wavelength in Eq. (7). Also, a higher field intensity and an increase of the dielectric constant is produced as the refractive index is increased [55–57].

According to Fig. 3 which represents the relationship between the resonance wavelengths and the refractive indices with and without rectangular defect in the cavity. It is clearly shown the maintained linearity between the resonance wavelengths with refractive index. Also, the achieved resonance wavelengths of MIM sensor with the presence of rectangular defect in cavity are greater than resonance wavelengths of MIM sensor without rectangular defect in cavity. According to Eq. (7) in the article, the resonant wavelength is proportional to the effective index. In other hand, based on the published article [58], the efective refractive index is correlated inversely with the width of MIM waveguide. Therefore, the resonant wavelength is inversely proportional with the width of MIM waveguide. Moreover, the equivalent air width in the metal is reduced which results in an increase in the resonant wavelength based on the aforementioned reasoning.

In Fig. 4 (a), the resonance wavelength is 1.46 μm for the structure without defect. However, when the tooth defect is presented there is no resonance at 1.46 μm wavelength as shown in Fig. 4b but for Fig. 4c, the structure is resonating at 1.92 μm. It is noticed the increase in the resonance wavelength when the tooth defect is presented.

More important is the obtained sensitivity of the two sensorial structures (slop of the two lines), it is clearly seen that the existence of rectangular defect in cavity results in increase of device sensitivity of 1943 nm/RIU compared to 1418 nm/RIU. In other words, the corresponding sensing resolution of 7.05×10^{-6} RIU is improved to 5.14×10^{-6} RIU with the presence of rectangular defect in cavity.

From Fig. 5, the larger the defect length is, the greater the resonance wavelength it is. In other words, the defect length L_c introduces a shift of resonance wavelength as shown in Fig. 5(a).

According to Fig. 5(b) all wavelength resonances are linear with respect to the refractive indices despite the increase in the defect length. Also, it is observed the shift in frequency resonances. More important, the greater the defect length from 50 nm to 125 nm is, the higher the sensitivity of the sensor it is. Hence, The best augmented sensitivity from 1831 nm/RIU to the best value of 2143 nm/RIU, i.e. sensing resolution of 4.67×10^{-6} RIU, can be achieved when the defect length $L_c = 125$ nm. However, a slight degradation in sensitivity is observed as the defect length increases further more than 125 nm. In Fig. 5(c) it is obviously seen the achieved linear improvements of the sensitivity with respect to the defect length L_c till its best value of 125 nm.

In Fig. 6(a), the structure with tooth defect, whose length is $L_c = 50$ nm, resonates at wavelength of 1.85 μm. when $L_c = 125$ nm there is no resonance at 1.85 μm wavelength as shown in Fig. 6b but the resonance is exhibited at resonance wavelength of 2.09 μm in Fig. 6c. It is also noticed the increase in the resonance wavelength when the tooth defect length is increased.

Previous results yield the best defect length of $L_c = 125$ nm. Thus, it is fixed for next analysis. From Fig. 7, the increase in defect width W_c from 10 to 40 nm is associated with an increase in resonance wavelength. In other words, the defect width W_c introduces a shift in resonance wavelength.

Further more, it is obseved a degradation in transmission level till the value − 17.1 dB as seen in Fig. 7(a); this degradation will be traeted in the next section. According to Fig. 7(b) the linearity of wavelength resonances with respect to the refractive indices is maintained in spit of the increase in the defect width. Besides, the shift in frequency resonances is also observed. However, more interesting result is the enhancement of sensor sensitivity by increasing the defect width where a sensitivity of 2602.5 nm/RIU, i.e. sensing resolution of 3.84×10^{-6} RIU, is achieved corresponding to defect width of 40 nm compared to sensitivity of 1580 nm/RIU which corresponds to the defect width of 10 nm. Furthermore, malfunction of the sensor is observed as defect width is increased more than 40 nm. In Fig. 7(c) it is clearly shown the achieved sensitivity with respect to defect widths W_c, the greater the defect width is, the better sensor performance is. It is conluded that the best defect width is 40 nm.

In Fig. 8(a), the structure with tooth defect, whose width is $W_c = 10$ nm, resonates at wavelength of 1.60 μm. when $W_c = 40$ nm

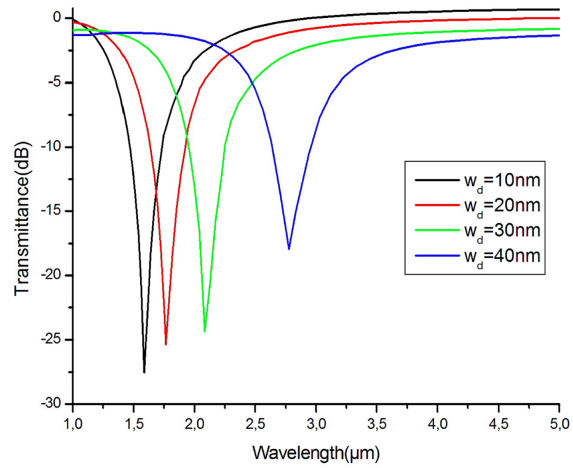

(a)

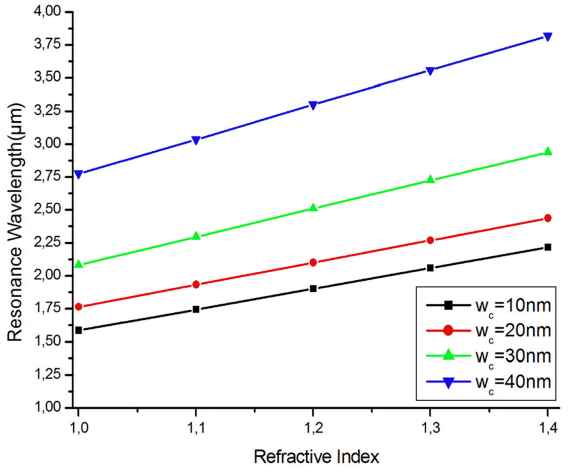

(b)

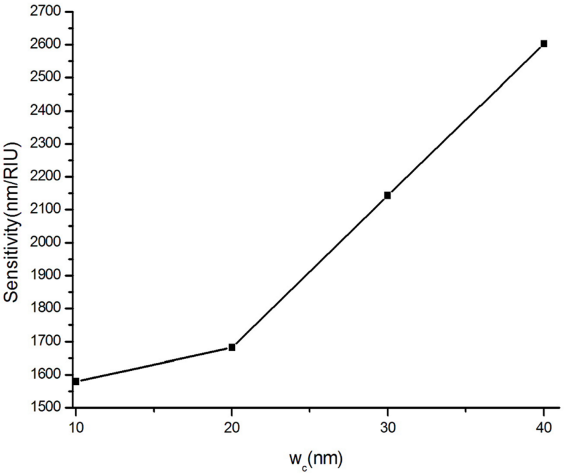

(c)

Fig. 7. Properties of MIM sensor coupled with rectangular defect in single cavity for various defect's rectangular width W_c = 10, 20, 30 and 40 nm with L_c = 125 nm (a) The transmission spectra of refractive index 1 as functions of W_c (b) The resonance wavelengths versus the refractive index for different W_c (c) The sensitivity versus defect's rectangular width W_c.

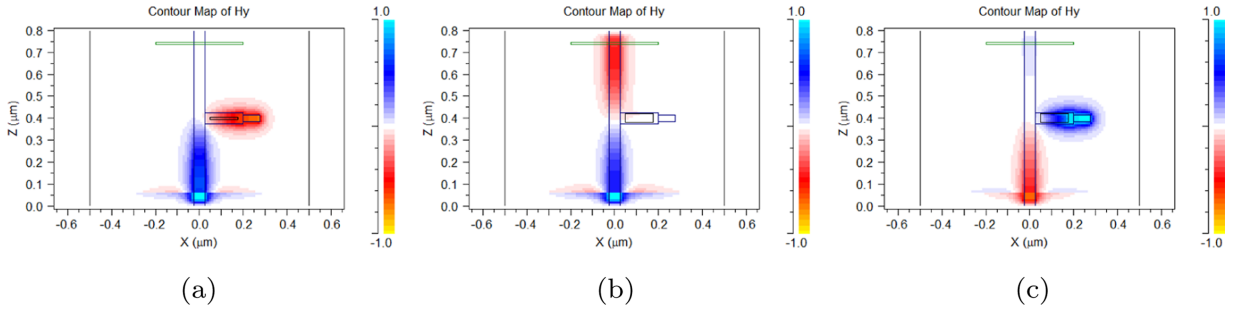

Fig. 8. The field distribution contours in the structure for (a) tooth defect length L_c = 125 nm, width length W_c = 10 nm at resonance wavelength 1.6 μm. (b) L_c = 125 nm, W_c = 40 nm at wavelength 1.6 μm. (c) L_c = 125 nm, W_c = 40 nm at resonance wavelength 2.79 μm.

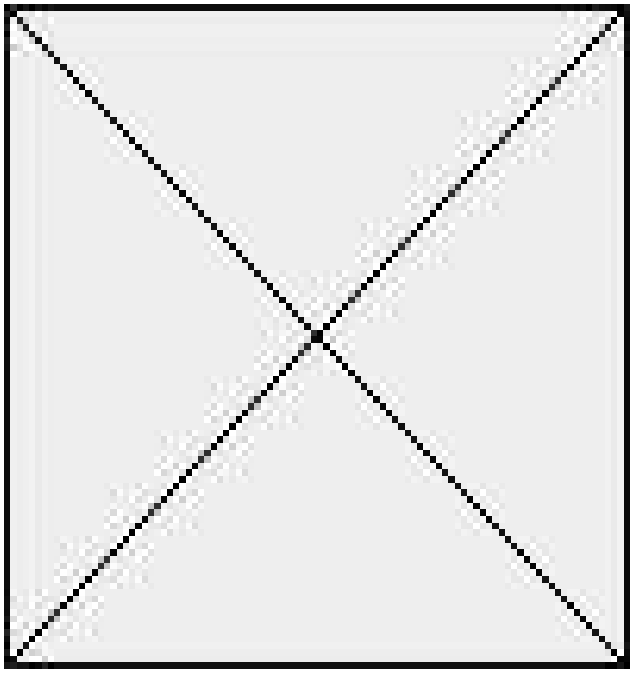

Fig. 9. 2-dimensional (2D) schematic of the presented metal-insulator-metal sensor coupled with double cavities with rectangular defect.

there is no resonance at 1.60 μm wavelength as shown in Fig. 8b but the resonance is presented at resonance wavelength 2.79 μm in Fig. 8c. It is also concluded the increase in the resonance wavelength when the tooth defect width is increased.

4. Design of enhanced sensor transmission

In this section, the treatment of previously reported degradation in tansmission level is conducted where the best dimensions of rectangular defect in cavity L_c = 125 nm and W_c = 40 nm achieved in previous section are fixed. A schematic of the proposed MIM sensor is shown in Fig. 9. As it can be seen, another double teeth and rectangular defect in cavity are added to the previously presented sensor with different distances of D = 0, 75, 150, 225, 300, 350 and 365 nm to old cavities.

5. Simulation results

Transmission spectra of the enhanced MIM sensor coupled with rectangular defect in double cavities for refractive index 1 with L_c = 125 nm and W_c = 40 nm and distance D = 0 nm is shown in Fig. 10 (a). The achievement in transmission level with no shift of resonance wavelength 2775 nm is a worthwhile as it is enhanced by 28.65% from − 17.1 dB to − 22 dB with nearby sensor sensitivity to previously presented structure. The effect of distance D is investigated at different values in the range 0 nm–365 nm with respect to sensor transmission and shown in Fig. 10(b). it is found that the transmission level is enhanced as the distance D is increased in the range of 0–300 nm but the enhancement of transmission level stops beyond 300 nm and becomes stable. In Fig. 11(a), the transmission spectra of the best presented structure with L_c = 125 nm, W_c = 40 nm and distance D = 300 nm is presented with the

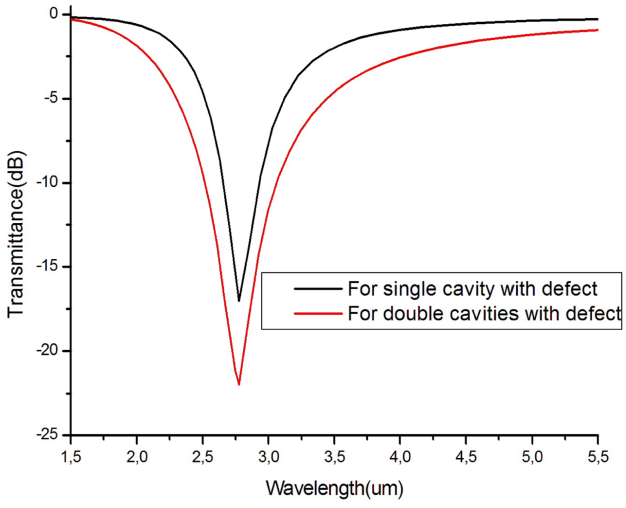

(a)

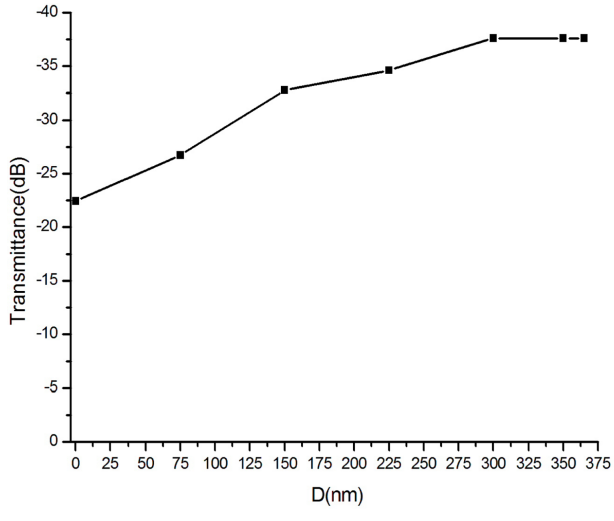

(b)

Fig. 10. (a)The transmission spectra of MIM sensor for single and double cavities with rectangular defect where L_c = 125 nm, W_c = 40 nm and D = 0 nm for n = 1 (b) The transmittance(dB) versus the distance D = 0, 75, 150, 225, 300, 350 and 365 nm and W_c = 40 nm for n = 1.

achieved linearity of sensor performance as shown in Fig. 11(b) which represents the resonance wavelength versus refractive indices.The highly designed sensitivity achieved in our proposed sensor with the improved transmission level affords extra features for designing real time on-chip optical sensors. Table 1 compares the sensitivity (S) for different reported MIM plasmonic sensors in literatures.

6. Conclusion

In this paper, a simple plasmonic refractive index sensor is proposed. The simplicity with sensing sensibility and transmission spectrum level which can be easily controlled by manipulating the structural parameters are the main advantages of the proposed structures. The reported MIM sensor establishes a transmission level of − 37.29 dB which is an enhanced value by 118.08% compared to the first design with the same improved sensitivity of 2602.5 nm/RIU. The simulations are performed based on 2D FDTD method. This compact structure can easily be employed for different useful sensors of temperature, pressure, humidity and concentration of chemicals based on the refractive index variations through proper designs.

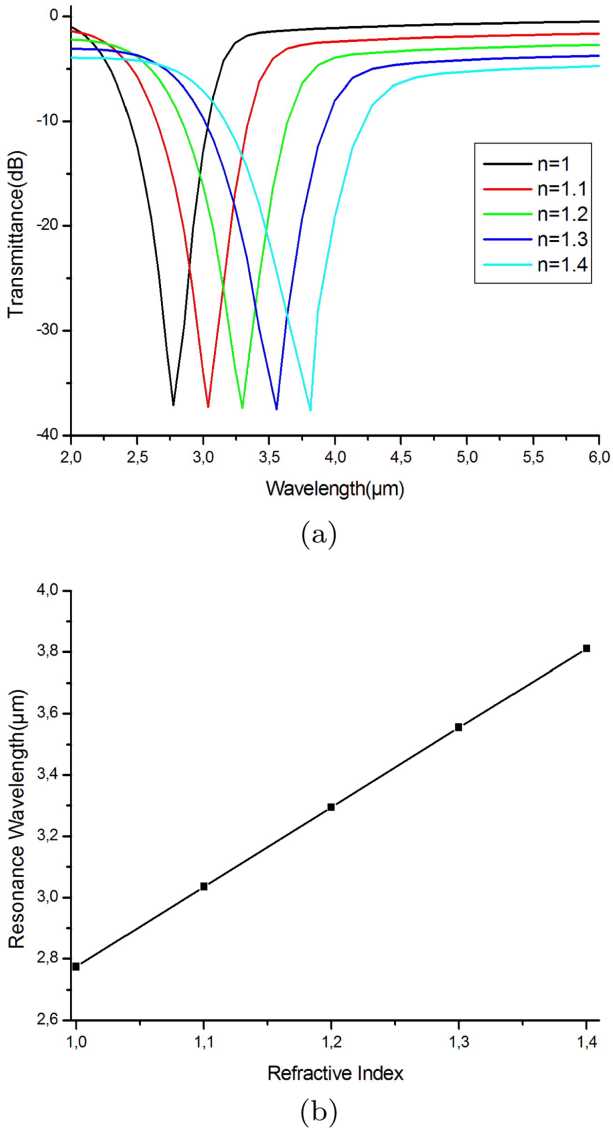

Fig. 11. (a) The transmission spectra of MIM sensor coupled with rectangular defect in double cavities for different refractive indices with L_c = 125 nm, W_c = 40 nm and D = 300 nm(b) The resonance wavelengths of MIM sensor coupled with rectangular defect in double cavities versus the refractive index with L_c = 125 nm, W_c = 40 nm and D = 300 nm.

Table 1
Sensitivity comparison of different sensor structures.

Reference	Sensitivity(*nm/RIU*)	Year
[59]	1602.5	2012
[60]	1160	2013
[61]	1562.5	2015
[62]	985	2016
[63]	2610	2016
[64]	4270	2016
[65]	1160	2018
In this work	2602.5	2019

Declaration of Competing Interest

None.

Acknowledgments

This work was supported by the Algerian Ministry of Higher Education and Scientific Research via funding through the PRFU project No. A25N01UN280120180001.

References

[1] J. Dong, W. Gao, Q. Han, Y. Wang, a. Qi, X. Yan, M. Sun, Plasmon-enhanced upconversion photoluminescence: mechanism and application, Rev. Phys. 4 (2019) 83–91, https://doi.org/10.1016/j.revip.2018.100026.
[2] Y.F.C. Chau, J.C. Jiang, C.T.C. Chao, H.P. Chiang, C.M. Lim, Manipulating near field enhancement and optical spectrum in a pair-array of the cavity resonance based plasmonic nanoantennas, J. Phys. D 49 (47) (2016) 475102.
[3] D.K. Gramotnev, S.I. Bozhevolnyi, Plasmonics beyond the diffraction limit, Nat. Photon. 4 (2) (2010) 83–91.
[4] V. Kaur, S. Singh, A dual-channel surface plasmon resonance biosensor based on a photonic crystal fiber for multianalyte sensing, J. Comput. Electron. 18 (1) (2019) 18–319, https://doi.org/10.1007/s10825-019-01305-7.
[5] S. Wang, X.Y. Wang, B. Li, H.Z. Chen, Y.L. Wang, L. Dai, R.F. Oulton, R.M. Ma, Unusual scaling laws for plasmonic nanolasers beyond the diffraction limit, Nat. Commun. 8 (2017) 1889.
[6] Y. Gao, G. Ren, B. Zhu, L. Huang, H. Li, B. Yin, S. Jian, Tunable plasmonic filter based on graphene split-ring, Plasmonics 11 (1) (2016) 291–296.
[7] Z. Vafapour, A. Zakery, New approach of plasmonically induced reflectance in a planar metamaterial for plasmonic sensing applications, Plasmonics 11 (2) (2015) 609–618.
[8] M. Kaboli, M. Akhlaghi, Investigating the optical AND gate using plasmonic nano-spheres, J. Comput. Electron. 15 (1) (2016) 295–300, https://doi.org/10.1007/s10825-015-0747-4.
[9] D. Etezadi, I.V. J. B. Warner, F.S. Ruggeri, G. Dietler, H.A. Lashuel, H. Altug, Nanoplasmonic mid-infrared biosensor for in vitro protein secondary structure detection, Light Sci. Appl. 6 (2017) 17029.
[10] M.F.O. Hameed, A.S. Saadeldin, E.M. Elkaramany, S.S. Obayya, Label-free highly sensitive hybrid plasmonic biosensor for the detection of DNA hybridization, J. Light. Technol. 35 (2017) 4851–4858.
[11] W. Kong, D. Wu, N. Hu, N. Li, C. Dai, X. Chen, Y. Suo, G. Li, Y. Wu, Robust hybrid enzyme nanoreactor mediated plasmonic sensing strategy for ultrasensitive screening of anti-diabetic drug, Biosens. Bioelectron. 99 (2018) 653–659.
[12] X. Li-Ping, W. Fa-Qiang, L. Rui-Sheng, Z. Shi-Wei, H. Miao, A high-sensitivity refractive-index sensor based on plasmonic waveguides asymmetrically coupled with a nanodisk resonator, Chin. Phys. Lett. 32 (7) (2015) 070701.
[13] M.R. Rakhshani, M.A. Mansouri-Birjandi, Dual wavelength demultiplexer based on metal-insulator-metal plasmonic circular ring resonators, J. Mod. Opt. 63 (2016) 1078–1086.
[14] T. Hu, H. Qiu, Z. Zhang, X. Guo, C. Liu, M. Rouifed, C. Littlejohns, G. Reed, H. Wang, A compact ultrabroadband polarization beam splitter utilizing a hybrid plasmonic y-branch, IEEE Photon. J. 8 (4) (2016) 4802209.
[15] H. Zhuang, F. Kong, K. Li, S. Sheng, Plasmonic bandpass filter based on graphene nanoribbon, Appl. Opt. 54 (2015) 2558–2564.
[16] M.R. Rakhshani, M.A. Mansouri-Birjandi, High sensitivity plasmonic sensor based on metal-insulator-metal waveguide and hexagonal-ring cavity with round-corners, IEEE Sens. J. 16 (2016) 3041–3046.
[17] Y.F.C. Chau, et al., Simultaneous realization of high sensing sensitivity and tunability in plasmonic nanos tructures arrays, Sci. Rep. 7 (1) (2017) 16817.
[18] Y.F.C. Chau, et al., Depolying tunable metal-shell/dielectric core nanorod arrays as the virtually perfect absorber in the near-infrared regime, ACS Omega 3 (7) (2018) 7508–7516.
[19] C.-H. Lai, Near infrared surface-enhanced raman scattering based on star-shaped gold/silver nanoparticles and hyperbolic metamaterial, Sci. Rep. 7 (2017) 5446.
[20] B. Xiao, et al., Topographically engineered large scale nanostructures for plasmonic biosensing, Sci. Rep. 6 (2016) 24385.
[21] J. Ye, Fabrication of metal nanostructures with programmable length and patterns using a modular DNA platform, Nano Lett. 19 (4) (2019) 2707–2714.
[22] F.Z. Zou, X. Pan, W. Luo, B. Yan, Multiple-channel plasmonic filter based on metal-Insulator-Metal waveguide and fractal theory, Plasmonics 12 (5) (2017) 1589–1594.
[23] S. Banerjee, In design and simulation of metal-insulator-metal nanoresonators for color filter applications, Proceeding of SPIE 9181, Light Manipulating Organic Materials and Devices, (2014), p. 918111.
[24] Z. Lu, R. Yang, R.A. Wahsheh, M.A.G. Abushagur, Nanoplasmonic couplers and modulators based on metal-insulator-metal structures, Proceeding of SPIE 7604, Integrated Optics: Devices, Materials, and Technologies, (2010).
[25] M.C. Onbasli, A.K. Okyay, Nanoantenna couplers for metal-insulator-metal waveguide interconnects, Proceeding of SPIE 7757, Plasmonics: Metallic Nanostructures and Their Optical Properties VIII, (2010).
[26] M. Kwon, J. Shin, J.H. Lee, Metal-insulator-silicon-insulator-metal waveguide splitters with large-arm separation, J. Lightwave Technol. 33 (18) (2015) 3843–3849.
[27] H. Zhao, Z. Li, D. Yuan, W. Li, Optical bistability with low intensity threshold in SPPs resonator multilayer nanostructure plasmonic filter with sub-waveguide coupled to vertical rectangular resonator structure, Optik - Int. J. LightElectron Opt. 127 (7) (2016) 3509–3512.
[28] J. Zhu, W. Xua, F. Deli, S. Song, Asymmetric SPP waveguide without sacrificing the size of subwavelength waveguide, Optik - Int. J. LightElectron Opt. 127 (12) (2016) 5092–5096.
[29] M. Bai, C. Wang, Tunable enhanced optical transmission in a metal-dielectric multilayer structured with annular aperture arrays, Optik - Int. J. LightElectron Opt. 124 (17) (2013) 2904–2908.
[30] T.S. Wu, Y.M. Liu, Z.Y. Yu, Y.W. Peng, C.G. Shu, H. Ye, The sensing characteristics of plasmonic waveguide with a ring resonator, Opt. Express. 22 (7) (2014) 7669–7677.
[31] K. Li, M.I. Stockman, D.J. Bergman, Self-similar chain of metal nanospheres as an efficient nanolens, Phys. Rev. Lett. 91 (2003) 227402.
[32] Z. Han, E. Forsberg, S. He, Surface plasmon bragg gratings formed in metal-insulator-metal waveguides, IEEE Photon. Technol. Lett. 19 (2007) 91–93.
[33] H. Gao, H. Shi, C. Wang, C. Du, X. Luo, Q. Deng, Y. Lv, X. Lin, H. Yao, Surface plasmon polariton propagation and combination in y-shaped metallic channels, Opt. Express 13 (26) (2005) 10795.
[34] T.W. Lee, S. Gray, Subwavelength light bending by metal slit structures, Opt. Express 13 (24) (2005) 9652.
[35] Z. Han, S. He, Multimode interference effect in plasmonic subwavelength waveguides and an ultra-compact power splitter, Opt. Commun. 278 (1) (2007) 199.
[36] H. Zhao, X. Guang, J. Huang, Novel optical directional coupler based on surface plasmon polaritons, Phys. E 40 (10) (2008) 3025.
[37] S. Kumar, L. Singh, S.K. Raghuwanshi, Design of plasmonic half-adder and half-subtractor circuits employing nonlinear effect in mach-zehnder interferometer, J. Comput. Electron 16 (1) (2017) 139, https://doi.org/10.1007/s10825-016-0927-x.
[38] S.A. Maier, Plasmonics Fundamentals and Applications, Springe, 2007.
[39] D.K. Gramotnev, S.I. Bozhevolnyi, Plasmonics beyond the diffraction limit, Nat. Photon. 4 (2) (2010) 83–91.
[40] T. Tang, Y. Zhang, W. Liu, X. He, Theoretical study of a refractive index sensor based on directional coupling between metal-insulator- metal waveguides, Optik-

Int. J. Light Electron Opt. 127 (4) (2016) 2149–2152.
[41] P. Pfeifer, U. Aldinger, G. Schwotzer, S. Diekman, P. Steinrucke, Real time sensing of specific molecular binding using surface plasmon resonance spectroscopy, Sens. Actuators B. 54 (1999) 166.
[42] H.F. Gai, J. Wang, Q. Tian, Modified debye model parameters of metals applicable for broadband calculations, Appl. Opt. 46 (12) (2007) 2229–2233.
[43] Al-mahmod, Numerical studies on a plasmonic temperature nanosensor based on a metal-insulator-metal ring resonator structure for optical integrated circuit applications, Photon. Nanostruct. - Fundam.Appl. 25 (2017) 52–57.
[44] N.T.R.N. Kumara, et al., Plasmonic spectrum on 1d and 2d periodic arrays of rod-shape metal nanoparticle pairs with different core patterns for biosensor and solar cell applications, J. Opt. 18 (11) (2016) 115503.
[45] Y.-F.C. Chau, C.T.C. Chao, H.J. Huang, Y.-C. Wang, H.-P. Chiang, M.N.S.M. Idris, Z. Masri, C.M. Lim, Strong and tunable plasmonic field coupling and enhancement generating from the protruded metal nanorods and dielectric cores, Results Phys. 13 (2019) 102290.
[46] J. Dionne, L. Sweatlock, H. Atwater, A. Polman, Plasmon slot waveguides: towards chip-scale propagation with subwavelength-scale localization, Phys. Rev. B. 73 (2006) 035407.
[47] P.B. Johnson, R. W. Christy, Optical constants of the noble metals, Phys. Rev. B. 12 (1972) 4370–4379.
[48] R. Zafar, M. Salim, Enhanced figure of merit in fano resonance based plasmonic refractive index sensor, IEEE Sens. J. 15 (11) (2015) 6313–6317.
[49] X. Zhang, M. Shao, X. Zeng, High quality plasmonic sensors based on fano resonance created through cascading double asymmetric cavities, Sensors 16 (2016) 1730.
[50] P.K. Wei, Y.C. Huang, C.C. chieng, F.G. Tseng, W. Fann, Off angle illumination induced surface plasmon coupling in subwavelength metallic slits, Opt. Express. 13 (26) (2005) 10784–10794.
[51] Q. Zh Aang, X.G. Huang, X.S. Lin, J. Tao, X.P. Jin, A subwave length coupler-type MIM optical filter, Opt. Express 17 (9) (2009) 7549–7555.
[52] L. Chen, Y. Liu, Z. Yu, D. Wu, R. Ma, Y. Zhang, H. Ye, Numerical analysis of a near-infrared plasmonic refractive index sensor with high figure of merit based on a fillet cavity, Opt. Express. 24 (9) (2016) 9975–9983.
[53] Rsoft Design Group, FullWAVE, Inc. 200 Executive Blvd. Ossining, NY 10562.
[54] A. Dolatabady, N. Granpayeh, V.F. Nezhad, A nanoscale refractive index sensor in two dimensional plasmonic waveguide with nanodisk resonator, Opt. Commun. 300 (2013) 265–268.
[55] Y.-F. Chau, Surface plasmon effects excited by the dielectric hole in a silver-shell nanospherical pair, Plasmonics 4 (4) (2009) 253–259, https://doi.org/10.1007/s11468-009-9100-8.
[56] Y.F. Chau, et al., Structurally and materially sensitive hybrid surface plasmon modes in periodic silver-shell nanopearl and its dimer arrays, J. Nanopart. Res. 15 (3) (2013) 1424.
[57] W. Yang, et al., Analysis of transmittance properties of surface plasmon modes on periodic solid/outline bowtie nanoantenna arrays, Phys. Plasmas 20 (6) (2013) 064503.
[58] Q. Zhang, X.-G. Huang, X.-S. Lin, J. Tao, X.-P. Jin, A subwavelength coupler-type MIM optical filter, Opt. Express 17 (9) (2009) 7549–7554.
[59] J.H. Zhu, X.G. Huang, J. Tao, X.P. Jin, X. Mei, Nanometeric plasmonic refractive index senor, Opt. Commun. 285 (2012) 3242–3245.
[60] S.-H. Kwon, Deep subwavelength-scal metal-insulator-metal plasmonic disk cavities for refractive index sensor, IEEE Photon. J. 5 (1) (2013) 4800107.
[61] Y.-Y. Xie, Y.-X. Huang, W.-L. Zhao, W.-H. Xu, C. He, A novel plasmonic sensor based on metal-insulator-metal waveguide with side-coupled hexagonal cavity, IEEE Photon. J. 7 (2) (2015) 4800612.
[62] F. chen, D. Yao, Realizing of plasmon fano resonance with a metal nanowall moving along MIMwaveguide, Opt. Commum. 369 (c) (2016) 72–78.
[63] M.R. Rakhsani, M.A. Mansouri-Birjandi, Utilizing the metallic nano-rods in hexagonal configuration to enhance sensitivity of the plasmonic racetrack resonator in sensing application, Plasmonic 12 (4) (2016) 999–1006.
[64] M.R. Rakhsani, M.A. Mansouri-Birjandi, High-sensitivity plasmonic sensor based on metal- insulator-metal waveguide and hexagonal-ring cavity, IEEE Sens. J. 16 (2016) 3041–3046.
[65] X. ZHANG, Q.I. Yunping, P. ZHOU, H. GONG, H.U. Bingbing, C. YAN, Refractive index sensor based on fano resonances in plasmonic waveguide with dual side-coupled ring resonators, Photon. Sens. 8 (4) (2018) 367–374.